

## RESEARCH ARTICLE

10.1002/2014JA020523

## Key Points:

- Saturn chorus intensity is binned in L, latitude, and local time
- Parametric fits of intensity versus frequency and latitude are determined
- Plasma injection regions can have significant chorus intensity

## Correspondence to:

J. D. Menietti,  
john-menietti@uiowa.edu

## Citation:

Menietti, J. D., T. F. Averkamp, J. B. Groene, R. B. Horne, Y. Y. Shprits, E. E. Woodfield, G. B. Hospodarsky, and D. A. Gurnett (2014), Survey analysis of chorus intensity at Saturn, *J. Geophys. Res. Space Physics*, 119, 8415–8425, doi:10.1002/2014JA020523.

Received 18 AUG 2014

Accepted 11 OCT 2014

Accepted article online 15 OCT 2014

Published online 30 OCT 2014

## Survey analysis of chorus intensity at Saturn

J. D. Menietti<sup>1</sup>, T. F. Averkamp<sup>1</sup>, J. B. Groene<sup>1</sup>, R. B. Horne<sup>2</sup>, Y. Y. Shprits<sup>3,4,5</sup>, E. E. Woodfield<sup>2</sup>, G. B. Hospodarsky<sup>1</sup>, and D. A. Gurnett<sup>1</sup>

<sup>1</sup>Department of Physics and Astronomy, University of Iowa, Iowa City, Iowa, USA, <sup>2</sup>British Antarctic Survey, Cambridge, UK, <sup>3</sup>Department of Earth and Space Sciences, University of California, Los Angeles, California, USA, <sup>4</sup>Department of Earth Atmospheric and Planetary Sciences, MIT, Cambridge, Massachusetts, USA, <sup>5</sup>Skolkovo Institute of Science and Technology, Moscow, Russia

**Abstract** In order to conduct theoretical studies or modeling of pitch angle scattering of electrons by whistler mode chorus emission at Saturn, a knowledge of chorus occurrence and magnetic intensity levels,  $P_B$ , as well as the distribution of  $P_B$  relative to frequency and spatial parameters is essential. In this paper an extensive survey of whistler mode magnetic intensity levels at Saturn is carried out, and Gaussian fits of  $P_B$  are performed. We fit the spectrum of wave magnetic intensity between the lower hybrid frequency and  $f_{ceq}/2$  and for frequencies in the interval  $f_{ceq}/2 < f < 0.9 f_{ceq}$  where  $f_{ceq}$  is the cyclotron frequency mapped to the equator. Saturn chorus is observed over most local times, but is dominant on the nightside in the range of  $4.5 < L < 7.5$ , with minimum power at the equator and peak power in the range of  $5^\circ < \lambda < 10^\circ$ . Saturn wave magnetic intensity averaged in frequency bins peaks in the range of  $10^{-5} < P_B < 10^{-4}$  nT<sup>2</sup> for  $0.4 < \beta < 0.5$  ( $\beta = f/f_{ceq}$ ). Gaussian fits of  $P_B$  with frequency and latitude are obtained for lower band chorus. Plasma injection regions are occasionally encountered with significant chorus power levels. Upper band chorus is seen almost exclusively within plasma injection regions, and the number of events is very limited, but when present, the average levels of  $P_B$  can be higher than the lower band chorus. The overall magnetic intensity contribution of the upper band, however, is insignificant relative to the lower band.

## 1. Introduction

Whistler mode chorus emission is known to be a significant source of electron energization and pitch angle scattering at Earth [cf. Baker *et al.*, 2013; Thorne *et al.*, 2013; Reeves *et al.*, 2013, and references therein]. Recent observations of Thermal Emission Imaging System and Van Allen Probes have greatly expanded the knowledge of the processes by which chorus emissions both fill the radiation belts and scatter or precipitate electrons. Similar processes have also been modeled at Jupiter [Horne *et al.*, 2008; Woodfield *et al.*, 2013, 2014], and comparative studies of chorus observations at Jupiter and Saturn have more recently been reported [cf. Hospodarsky *et al.*, 2012; Menietti *et al.*, 2012; Shprits *et al.*, 2012]. Hospodarsky *et al.* [2008] have reported the initial chorus observations of the Cassini Radio and Plasma Wave Science (RPWS) investigation and a survey mapping of the locations of the emissions within the Kronian magnetosphere encountered after the first 50 orbits. The authors reported chorus in two general regions. The most common observations were of chorus propagating away from the region of Saturn's magnetic equator. At the time, chorus was only observed in the lower band ( $f < f_c/2$ ), with no apparent correlation with latitude or local time. Menietti *et al.* [2014] have reported on latitudinal variations of Saturn chorus for the special case of Cassini orbits along nearly constant L shells near the magnetic equator. The second region of chorus observations reported by Hospodarsky *et al.* [2008] was in association with plasma injection (depletion) regions.

The plasma depletion (or injection) regions observed on Cassini have been discussed in the past [Hill *et al.*, 2005; Burch *et al.*, 2005; Menietti *et al.*, 2008; Rymer *et al.*, 2009]. These regions are believed to result from the plasma interchange instability at both Jupiter and Saturn. They are seen in rapidly rotating planets and result from the inward transport of hot, tenuous plasma and outward transport of dense, cold plasma. At Saturn, Chen and Hill [2008] found them to occur from 5% to 10% of the time in the region  $5 < L < 10$ . A more recent survey of Kennelly *et al.* [2013], focusing on young events (which are those most often observed by RPWS), largely agree with this distribution in L. Chorus emission has been observed in these regions in both the upper and lower bands, and some of the most intense chorus is observed within these regions [Hospodarsky *et al.*, 2008; Menietti *et al.*, 2008].

The importance of chorus emission in the acceleration of electrons at Jupiter has been demonstrated, as noted before, but it is believed that high ratios of plasma to cyclotron frequency in the Saturn magnetosphere may make the role of chorus at Saturn less efficient [Shprits *et al.*, 2012]. In order to conduct better modeling of pitch angle scattering of electrons by chorus emission at either Jupiter or Saturn, a knowledge of chorus occurrence

and intensity levels at the outer planets is essential, as well as the distribution of this power with respect to frequency and spatial coordinates. In this paper an extensive survey of the whistler mode chorus magnetic intensity levels at Saturn is conducted, similar to terrestrial chorus surveys performed by *Meredith et al.* [2012] for instance, and Gaussian fits to the intensity are performed which should aid in theoretical chorus simulations and modeling at Saturn. We acknowledge that the emission we study in this work is whistler mode but not necessarily chorus. Some of this emission is likely to be whistler mode hiss [*Thorne et al.*, 1973; *Gurnett et al.*, 2010] rather than chorus. We generally refer to the emission as chorus to conform with previous similar studies [cf. *Hospodarsky et al.*, 2008, 2012; *Meredith et al.*, 2012; *Li et al.*, 2011].

## 2. Methodology

The general scheme for conducting the chorus survey at each planet was to introduce spatial bins in magnetic L shell (L), magnetic local time, and magnetic latitude ( $\lambda$ ). For this survey, because of the near alignment of the magnetic and spin axes, the magnetic local time and local time were considered equal. Whistler mode chorus is assumed to be generated close to the magnetic equator and to propagate close to the magnetic field ( $k \cdot B_{\text{wave}} \sim 0$ ). The frequency spectrum for chorus was determined for the upper and lower bands normalized to the cyclotron frequency mapped to equator,  $f_{\text{ceq}}$ , ranging over  $f_{\text{lh}} < f < f_{\text{ceq}}/2$  and  $f_{\text{ceq}}/2 < f < f_{\text{ceq}}$ , where  $f_{\text{lh}}$  is the lower hybrid frequency. The lower band chorus is divided into five frequency bins and the upper band into three frequency bins. We introduce relative frequency,  $\beta_i = f_i/f_{\text{ceq}}$ , where  $f_i$  is the center frequency of the frequency bin,  $\Delta\beta_i$ . For the lower band, we define  $f_{\text{lh}}/f_{\text{ceq}} < \Delta\beta_1 < 0.1$ ,  $0.1 < \Delta\beta_2 < 0.2$ ,  $0.2 < \Delta\beta_3 < 0.3$ ,  $0.3 < \Delta\beta_4 < 0.4$ , and  $0.4 < \Delta\beta_5 < 0.5$ , while for the upper band, we define  $0.5 < \Delta\beta_6 < 0.6$ ,  $0.6 < \Delta\beta_7 < 0.7$ , and  $0.7 < \Delta\beta_8 < 1$ . The wave magnetic intensity is proportional to  $P_B = B^2(nT^2)$ . From the measured magnetic spectral density,  $\chi(f)$ , in units of  $nT^2/\text{Hz}$ , over a range of frequencies, we determine  $B^2(\beta_i)$  (measured in  $nT^2$ ) by integration over the frequency channels within  $\Delta\beta_i$  for a time step,  $\Delta\tau$  (typically 1 min), the sum of these integrations we call  $P_{B_i}$ . The spacecraft position (L,  $\lambda$ , and local time (LT)) at each time step,  $\Delta\tau$ , is always recorded. When seeking  $P_B(\beta)$ , we calculate the mean value of  $P_B$  within any chosen spatial bin ( $\Delta L$ ,  $\Delta LT$ , and  $\Delta\lambda$ ) by averaging all  $P_{B_i}$  within that spatial bin during the total integration time (the sum of  $\Delta\tau$ ). For a specific  $\Delta L$ , by calculating averages over all values of LT, and all values of  $\lambda$ , we can then fit  $P_B(\beta)$  to a Gaussian of the form shown in equation (1) and determine the fitting parameters  $P_o$ ,  $\beta_o$ , and  $w$ .

$$P_B(\beta) = P_o \exp\left\{-\frac{(\beta - \beta_o)^2}{w^2}\right\} \quad (1)$$

The functional form of equation (1) has been used by *Glauert and Horne* [2005], *Shprits et al.* [2006], and *Glauert et al.* [2014] among others.

We calculate the value of  $P_B$  per spectrum,  $P_{B_s}$ , by summing all the  $P_{B_i}$  for either the lower or upper bin for each  $\Delta\tau$ . If we wish to obtain  $P_B$  for a specified spatial range, we obtain the mean of all  $P_{B_s}$  within that spatial range during the total integration time (the sum of all  $\Delta\tau$ ). For instance, to obtain  $P_B(\lambda)$ , we calculate these mean values within a specific  $\Delta L$  for all values of LT and for all values of  $\lambda$  within each bin of latitude,  $\Delta\lambda$ . It is then possible to fit to the functional form shown in equation (2)

$$P_B(\lambda) = P_o \exp\left\{-\frac{(\lambda - \lambda_o)^2}{w^2}\right\}. \quad (2)$$

For each relative frequency bin,  $\Delta\beta_i$ , there may be several to perhaps 10 actual frequency steps or channels. For each of these frequency steps, there may be one to four spectral density values within the time step  $\Delta\tau$  (1 min). The median is taken of these (typically) one to four values at each actual frequency step. This is the only time a median value is calculated to limit outliers. At all other times, a mean average is obtained. For calculations of  $P_B$  versus  $\beta$ , we always obtain the mean or average of all  $P_{B_i}$  for each relative frequency bin within a spatial bin. For calculations of  $P_B$  versus spatial coordinates, we always obtain the mean or average of all  $P_{B_s}$  for either the lower or upper bin within a spatial bin as required for the quasi-linear calculation of the scattering rates [*Kenel and Engelmann*, 1966].

## 3. Models and Data Constraints

In order to perform the mapping to the equator, we have used the Z3 zonal harmonic model [*Connerney et al.*, 1982, 1983; *Acuña et al.*, 1983] for the Saturn magnetic field. The plasma density was measured locally by observation of the upper hybrid resonance,  $f_{\text{uh}} = \sqrt{f_p^2 + f_c^2}$ , where  $f_p$  is the local plasma frequency. However,

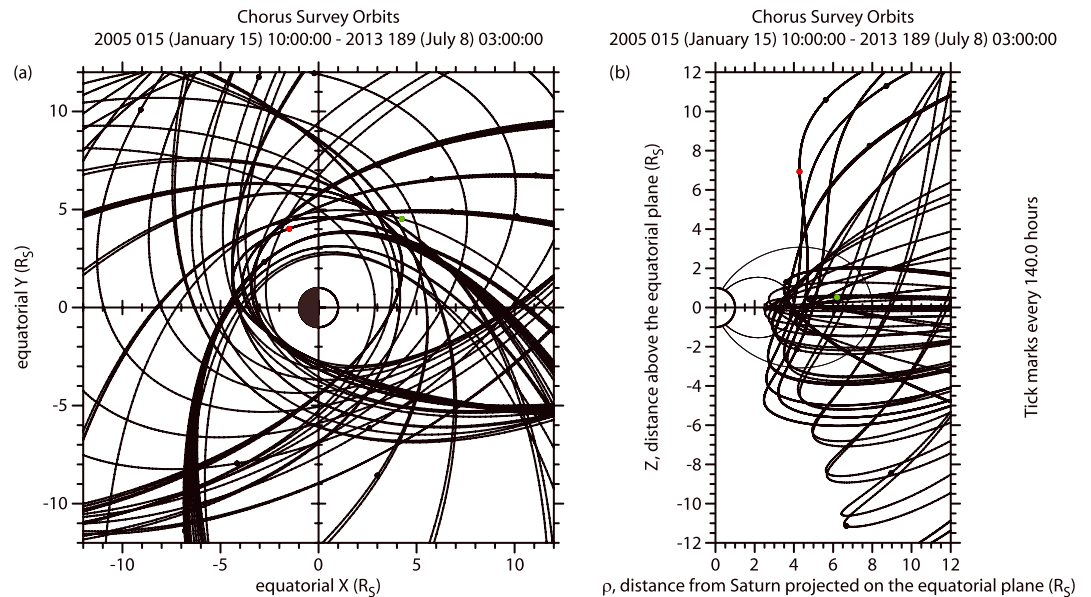


**Figure 1.** Segments of the Cassini orbits in the (a) equatorial ( $x$ - $y$ ) plane and in the (b)  $\rho$ - $z$  plane. The plots are limited to  $12 R_S$  in each coordinate.

often the upper hybrid resonance was not observed, so we have used the interpolated values of the Saturn plasma density model of *Persoon et al.* [2009] for Saturn's inner magnetosphere. The model values of the magnetic field and density at the equator were scaled by the local measured values when available.

The wave magnetic spectral density values were obtained at Saturn from the Radio and Plasma Wave Science (RPWS) instrument [*Gurnett et al.*, 2004]. This complex instrument includes three low-time resolution receivers, for low, medium, and high-frequency measurements: LFR (1–26 Hz), MFR (24 Hz–12 kHz), and HFR (3.5 kHz–16 MHz). For this study we have used the MFR data. There are three approximately orthogonal electric antennas (10 m) and three orthogonal search coils for magnetic measurements. The MFR usually toggles between the  $E_x$  and  $B_x$  antennas every 32 s (16 s each),  $\Delta f/f \sim 7\%$ . Examples of chorus emission data obtained from the MFR are shown as spectrograms in Figures 5, 6, and 7 of *Menietti et al.* [2012].

To avoid spacecraft and instrumental interference as well as natural wave interference, a number of constraints were placed on the data analyzed in this survey. Among the more important for the Cassini RPWS data are as follows:

1. Limit latitude to  $\lambda < 25^\circ$  to avoid intense auroral hiss emission. Auroral hiss emission is often observed at higher latitudes as seen in Figures 2–4 of *Gurnett et al.* [2010].
2.  $P_B < 6 \times 10^{-3} \text{ nT}^2$  for each  $\beta$  bin ( $\Delta\beta_i$ ) at a time step to avoid extraneous noise spikes and interference. Noise spikes include bursts of intense emission which vary in bandwidth but can be over 1 kHz. They are not natural and are likely due to spacecraft or instrumental interference.
3. Parameter  $f_{\min} = 200 \text{ Hz}$  to avoid “reaction wheel” noise. This is due to special spacecraft gyros that are essential for guidance and attitude control. This minimum frequency supersedes  $f_{lh}$ , if  $f_{lh} < 200 \text{ Hz}$ .
4. Parameter  $\chi(f) > 4 \times 10^{-8} \text{ nT}^2/\text{Hz}$  ( $\chi(f)$  = magnetic power spectral density) to avoid background noise (i.e., harmonics of reaction wheels).

### 3.1. Data Times

The data for the Saturn survey were obtained over approximately 7.5 years from 15 January 2005 to 8 July 2013. In Figure 1, we display plots of the orbits in the equatorial ( $x$ - $y$ ) plane and the  $\rho$ - $z$  plane. Each plot is confined to  $12 R_S$  ( $R_S$  = Saturn radius). These plots together provide a sense of the overall spacecraft coverage. The Cassini spacecraft was in equatorial orbits for slightly over one half of the time, while the remaining fraction of the time has been at higher inclination orbits visiting latitudes up to  $\sim 70^\circ$ .

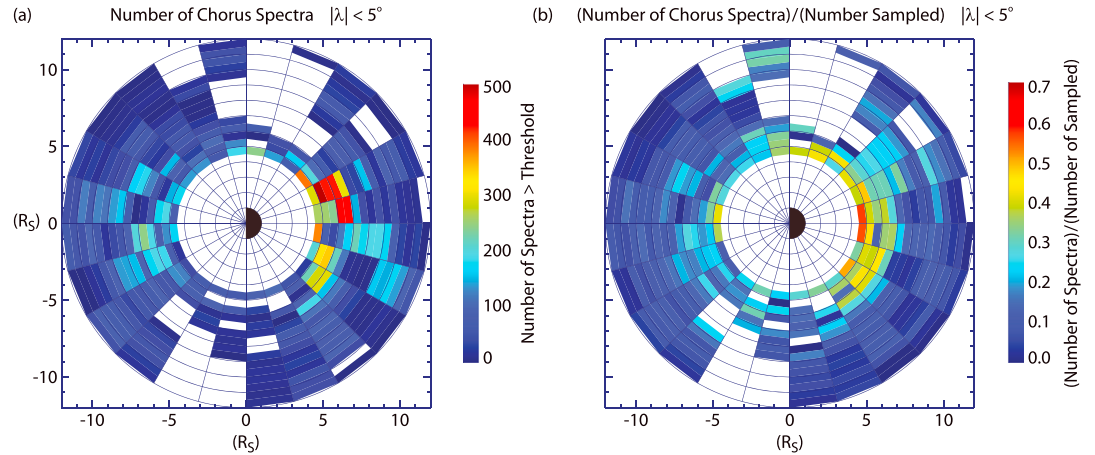


**Figure 2.** The equatorial plane ( $|\lambda| < 5^\circ$ ) divided into spatial bins of L shell and local time, with  $\Delta L = 0.5$  and  $\Delta LT = 1$  h. For lower band, we depict (a) the number of spectra of observed chorus in each bin and (b) the ratio of number of chorus spectra observed,  $N_s$ , relative to the number of sampled spectra,  $N_t$ , in each bin, or occurrence probability of Saturn chorus in the equatorial region.

### 4. Saturn Magnetic Intensity Surveys

#### 4.1. Lower Band

We first consider the lower band chorus. In Figure 2, we display the equatorial plane ( $|\lambda| < 5^\circ$ ) divided into spatial bins of L shell and local time, with  $\Delta L = 0.5$  and  $\Delta LT = 1$  h. In Figure 2a, we depict the number of spectra of

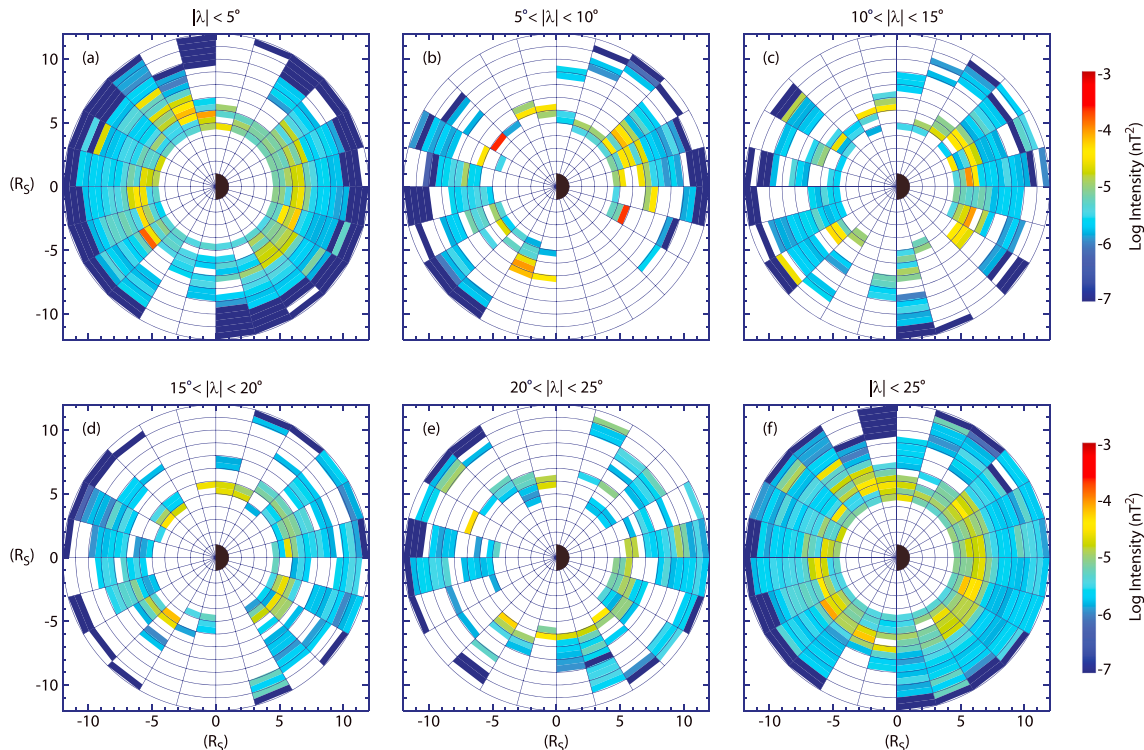


**Figure 3.** Average lower band spectral intensity measured per spatial bin in  $5^\circ$  latitude steps ( $\Delta\lambda = 5^\circ$ ) over the range of  $0 < |\lambda| < 25^\circ$ . Auroral hiss is frequently observed for  $|\lambda| > 25^\circ$ , and this range is therefore not sampled.

A-D14-053-1

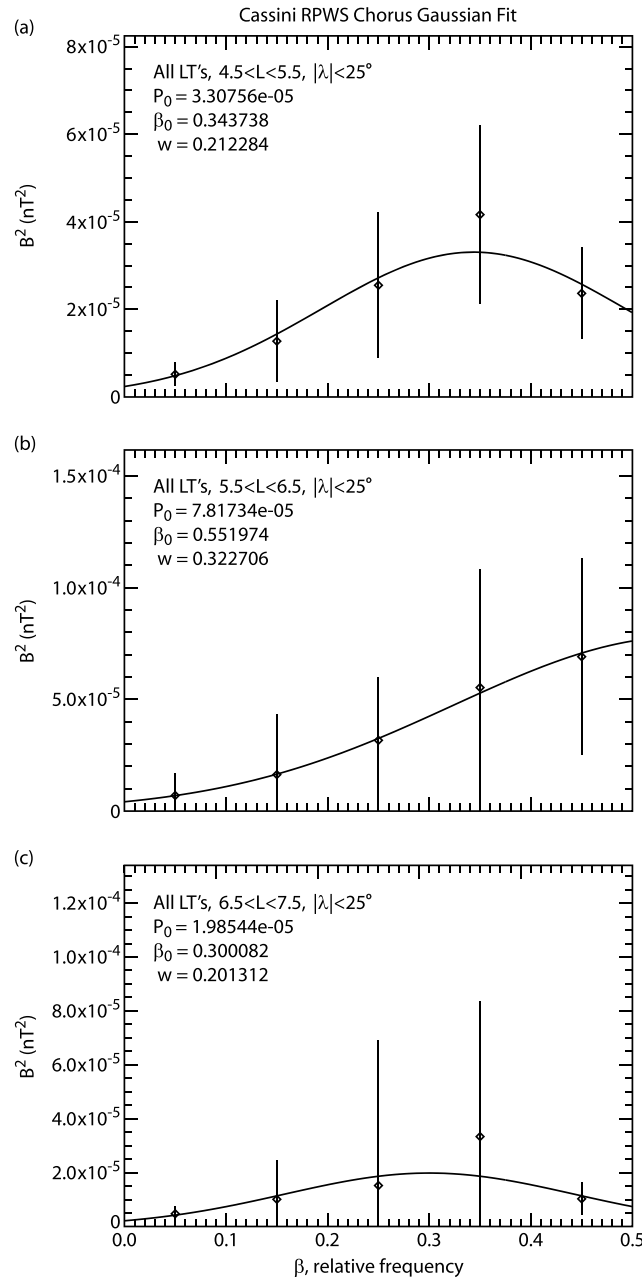


**Figure 4.** Least squares fits to equation (1) with  $\beta = ff_{ceq}$ . For each range of L, we display the average chorus intensity for all spectra within a spatial bin that includes all local times and  $|\lambda| < 25^\circ$ . The values of the fitting parameters for equation (1) are listed on each plot.

local times. In the analyses that follow (fitting of data and integrations versus L shell), we will not use the bins depicted in Figure 3, but we will perform averages of  $P_{Bi}$  and  $P_{Bs}$  over much larger bins to avoid skewing the results with bins containing few points.

As discussed earlier, from the data we can construct least squares fits to equation (1). We select a range of L and average  $P_B$  for all spectra within a spatial bin that includes all local times and  $|\lambda| < 25^\circ$ . Figure 4 shows the results for the three ranges of L, with the values of the fitting parameters listed on each plot. For  $4.5 < L < 5.5$ , we find  $P_0 = 3.31 \times 10^{-5} \text{ nT}^2$ ,  $\beta_0 = 0.344$ , and  $w = 0.212$ , while for  $6.5 < L < 7.5$ , we find  $P_0 = 1.99 \times 10^{-5} \text{ nT}^2$ ,  $\beta_0 = 0.30$ ,

observed chorus in each bin, with one bin slightly exceeding 500. In Figure 2b, we show the ratio of the number of chorus spectra observed,  $N_s$ , relative to the number of sampled spectra,  $N_t$ , in each bin for the equatorial region. This is the occurrence probability of Saturn chorus. During each time step,  $\Delta\tau$ , all relative frequency bins,  $\beta_i$ , are sampled, and a value of intensity,  $P_{Bs}$ , is determined.  $N_s$  is the number of time steps containing intensity levels that satisfy the four data constraints above for the lower band in each spatial bin of Figure 2. The range of  $N_s/N_t$  is from 0 to  $\sim 0.6$  for  $4.5 < L < 6$ . The ratio is highest in the approximate range of  $21 \text{ h} < \text{LT} < 26 \text{ h}$  (02 h). Both  $N_s$  and  $N_t$  fall off rapidly with latitude, since most of the Cassini orbits were near the equatorial plane. In Figure 3, we display the average value of  $P_B$  per spectrum,  $P_{Bs}$ , measured per spatial bin for latitude steps ( $\Delta|\lambda| = 5^\circ$ ) over the range of  $0 < |\lambda| < 25^\circ$ . Auroral hiss is frequently observed for  $|\lambda| > 25^\circ$ , and this range is therefore not sampled. The distribution of chorus power shows no particular dependence on local time (LT) but is somewhat patchy in the L-LT plane. The greatest occurrence of chorus is seen near the equator, but the highest intensity levels are above the equator in the range of  $\sim 5^\circ < |\lambda| < 10^\circ$ . Contour plots (Figures 3a–3e) in the L-LT plane are shown at a high resolution and display patchiness (particularly Figures 3b–3e), where there are few data points. Figure 3f depicts  $P_{Bs}$  averaged over each  $\Delta L$  and at all latitudes in the range of  $0 < |\lambda| < 25^\circ$ , displaying a ring of chorus emission in the approximate range of  $4.5 < L < 7.5$ . Even though the occurrence probability of chorus is higher on the nightside (Figure 2b), the average intensity distribution is not so localized, indicating that strong chorus events occur at all

A-D14-054-1

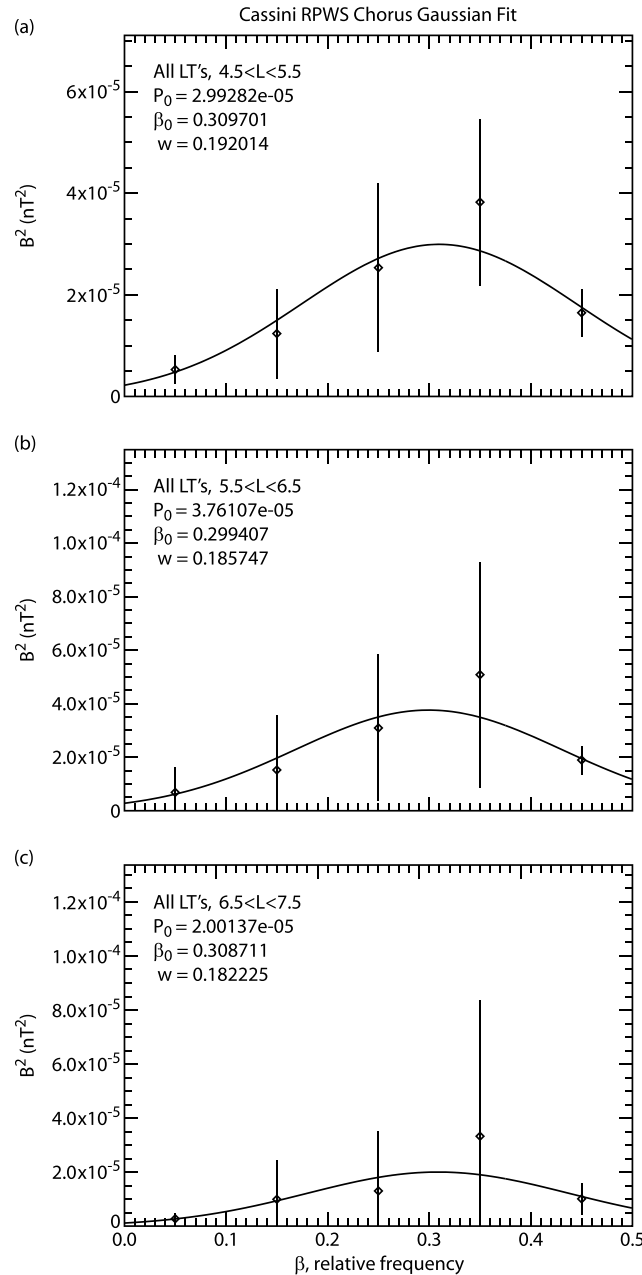


**Figure 5.** Chorus intensity versus  $\beta$  with new more severe intensity constraints, eliminating plasma injection regions with intense chorus. Compared to Figure 4, the intensity levels are lower and the peak power is not in the highest  $\beta$  bin for  $5.5 < L < 6.5$ .

intensity, including the most intense plasma injections,  $P_{oi}$ , to average intensity without these injections,  $P_o$ , for each range of L shell is listed in Table 1, indicating that plasma injections with significant chorus intensity levels can increase the total intensity in the range of  $5.5 < L < 6.6$  by a factor of ~2.

**Table 1.** Comparison of Chorus Intensity Including Intense Injections

	4.5 < L < 5.5	5.5 < L < 6.6	6.5 < L < 7.5
$P_{oi}/P_o$	1.11	2.08	0.992

and  $w = 0.20$ . The largest intensity is seen for  $5.5 < L < 6.5$  with  $P_o = 7.82 \times 10^{-5} nT^2$ ; however, the peak of the Gaussian fit occurs for  $\beta > 0.5$  as indicated on the plot. The error bars are determined from the variance of points in each bin of  $\beta$ . The large values of intensity for  $0.4 < \beta < 0.5$  in Figure 4b differ from Figures 4a and 4c. At Earth, typical chorus bands peak near  $\beta \sim 0.3$  [cf. Santolík et al., 2003]. Within plasma injection regions, however, observations indicate that chorus emissions can be at higher values of  $\beta$  and  $P_B$  [i.e., Hospodarsky et al., 2008; Menietti et al., 2008, 2012]. We therefore investigate the influence of plasma injection regions on the chorus data below.

Since, as noted above, injection regions sometimes display much larger levels of chorus intensity, we apply more stringent constraints on the maximum power levels in each bin of  $\beta$ . By examination, we determined that a more stringent level of  $P_B < 1 \times 10^{-3} nT^2$  for each  $\beta$  bin at a time step eliminates those few injection regions with significant chorus intensity levels while preserving almost all chorus outside of injection regions. However, chorus emission from injection regions with lower values of  $P_B$  would not be affected. We add here that a scheme to isolate plasma injection regions based on density depletions would not have been feasible because of the large range of values of  $f_p/f_c$  for each plasma injection. In fact, some plasma injection regions display an increase in the ratio of  $f_p/f_c$ . In Figure 5, we display plots of  $P_B$  versus  $\beta$  with these new more severe power constraints. Two things become apparent; the magnetic intensity levels are lower, and the peak intensity is not in the highest lower band  $\beta$  bin for  $5.5 < L < 6.5$ . The ratio of average

A-D14-055-1

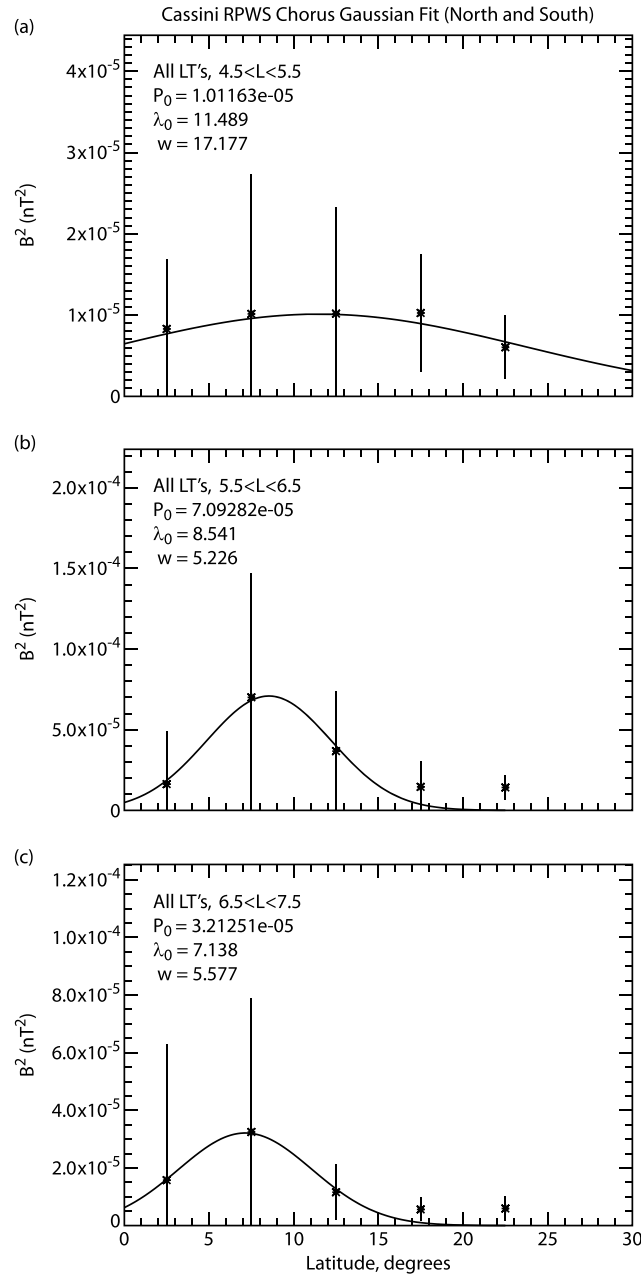


**Figure 6.** The latitudinal distribution of average chorus intensity (including all plasma injection regions). For each range of L, the spatial bin also includes all local times for successive latitude ranges,  $\Delta|\lambda| = 5^\circ$ .

For the remainder of our analyses, we apply the less restrictive intensity constraints, allowing the inclusion of all plasma injection regions. Next we obtain the latitudinal distribution of chorus intensity by selecting a range of L and averaging the chorus intensity for all spectra within a spatial bin that includes all local times and successive  $5^\circ$  bins in  $|\lambda|$ . We then fit the data to equation (2). The results are shown in Figure 6 for the same three ranges of L. For  $4.5 < L < 5.5$ , the chorus intensity shows small variation in  $\lambda$ , whereas for  $5.5 < L < 6.5$ , the chorus intensity peaks near  $\lambda = 8.5^\circ$  at  $P_0 = 7.1 \times 10^{-5} \text{ nT}^2$ , and for  $6.5 < L < 7.5$ , the chorus intensity peaks near  $\lambda = 7.1^\circ$  at  $P_0 = 3.2 \times 10^{-5} \text{ nT}^2$ . The error bars are determined by the variance of the points within the spatial bins. Finally, in Figure 7, we plot  $P_B$  averaged over all local times and latitudes for each  $\Delta L = 1$  in the range of  $4.5 < L < 7.5$ , showing the confinement of chorus intensity in L.

#### 4.2. Upper Band Chorus

We perform a similar analysis on the chorus upper band emission. In Figure 8, we show the number of spectra of observed upper band emission in each bin (Figure 8a) and the average intensity of upper band chorus per spatial bin in the equatorial plane (Figure 8b). The bin size is the same as for Figure 2. Only one event of upper band chorus was observed for  $|\lambda| > 5^\circ$ , so higher latitudes are not displayed. The number of observed spectra of upper band chorus are extremely few as seen in Figure 8a. The occurrences of upper band chorus are scattered in LT and are almost all located in injection regions. Each case was examined by eye, and only three were clearly not associated with an injection region. No occurrences were observed for  $L > 8$ . Figure 8 should not be

compared to survey maps of the distribution of plasma injection regions [cf. *Chen and Hill, 2008; Kennelly et al., 2013*], because only a percentage of plasma injection regions contain upper band chorus. We plot the average chorus intensity versus  $\beta = f/f_{ceq}$  in Figure 9. For this plot, we have averaged the spectral intensity over the full range of  $4.5 < L < 8.0$ , instead of for three distinct ranges of L as in Figure 4 for the lower band, because of the small number of data points. For  $0.5 < \beta < 0.6$ , there were 66 points; for  $0.6 < \beta < 0.7$ , there were 12 points; and there were only 4 points for the highest bin of  $\beta$ , so no Gaussian fits were obtained. In Figure 10a, we plot the average chorus intensity versus L (averaged in the same manner as the lower band in Figure 7), and it is seen that the intensity levels are higher than those for the lower band, but there is a paucity of source points for

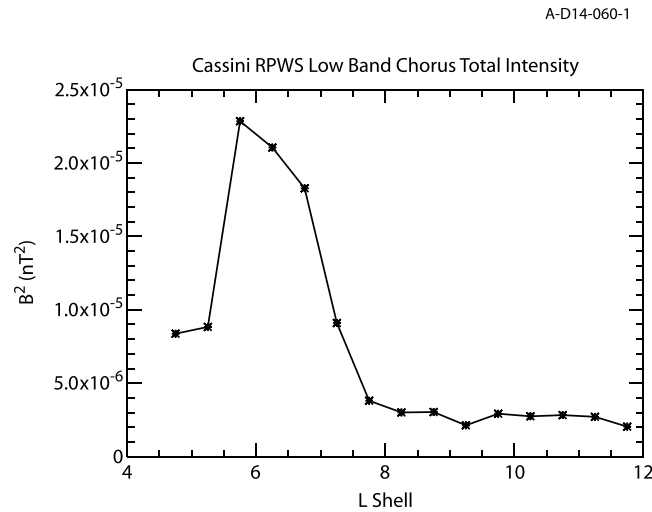


**Figure 7.** Chorus intensity averaged over all local times and latitudes for each  $\Delta L = 1$  in the range of  $4.5 < L < 7.5$ , showing the confinement of chorus power in L.

the upper band. Because of the few numbers of spectra of upper band chorus, a better sense of the total average intensity of both upper and lower bins is obtained by calculating  $P_{l,u}$ , the average frequency-integrated magnetic intensity for both chorus bands plotted versus L in Figure 10b. In Figure 11, we plot the average lower band magnetic intensity (cross) and  $P_{l,u}$  (circles) versus L. The two curves are nearly identical, indicating that the upper band contributes little total intensity compared to the lower band. The curves of  $P_{l,u}$  versus latitude are virtually identical to those shown in Figure 6 for the lower band only and are not shown.

### 5. Summary and Conclusions

These results provide the first comprehensive survey of plasma chorus

magnetic intensity at Saturn, with source regions sorted in L,  $\lambda$ , and LT, and mapped over the frequency range of  $f_{lh} < f < f_{ceq}$  (when available), using realistic magnetic field and plasma density models. The lower band chorus intensity levels have been fit to Gaussians in  $\beta$  and in  $\lambda$ , providing important information for theorists and modelers.

Saturn chorus occurrence is variable but dominant on the nightside in the range of  $4.5 < L < 7.5$  with typical  $\beta$  values of perhaps 0.3 to 0.4 and peak values approaching 0.6. Nevertheless, the average chorus intensity is rather evenly distributed in local time, so significant episodes of chorus occur at all local times. The highest chorus intensity levels occur in the subrange of  $5.5 < L < 6.5$ , notably not at the equator but in the range of  $5^\circ < |\lambda| < 10^\circ$ , falling off rapidly for  $|\lambda| > 15^\circ$ . Gaussian fits of intensity with frequency indicate that lower band chorus power peaks in the range of  $0.4 < \beta < 0.5$  at a value of  $\sim 8 \times 10^{-5} \text{ nT}^2$  for the range of  $4.5 < L < 6.5$ . Intense chorus is sometimes observed within a small number of plasma injection regions. These few, scattered injection regions, randomly seen (and probably more often missed) by Cassini, are observed to approximately double the average power in the range of  $5.5 < L < 6.5$ . By isolating from the survey those few

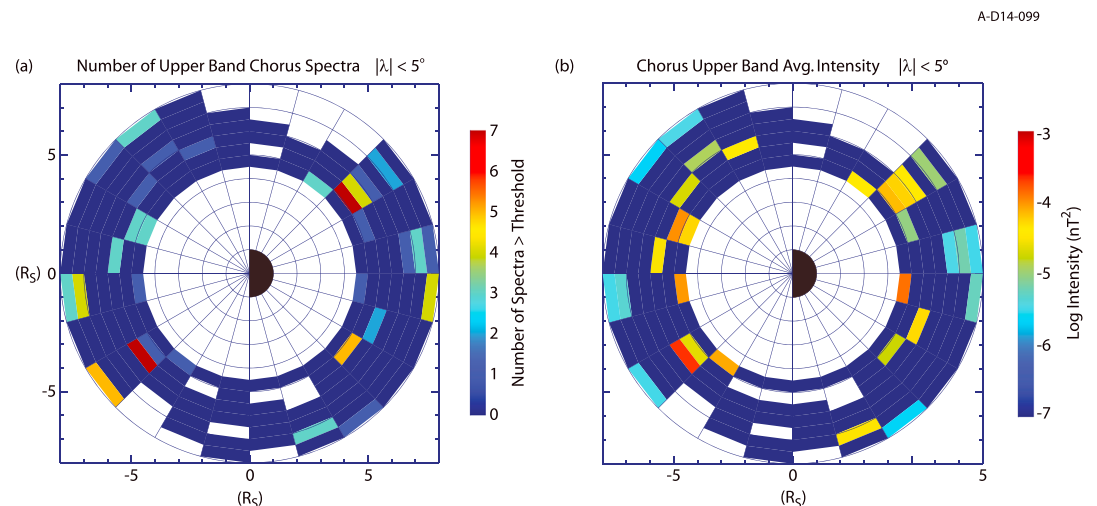


**Figure 8.** For the upper band chorus in the equatorial plane, we display (a) the number of observed spectra in each bin and (b) the average intensity in each bin. The occurrences of upper band chorus are almost all in injection regions.

A-D14-062-1

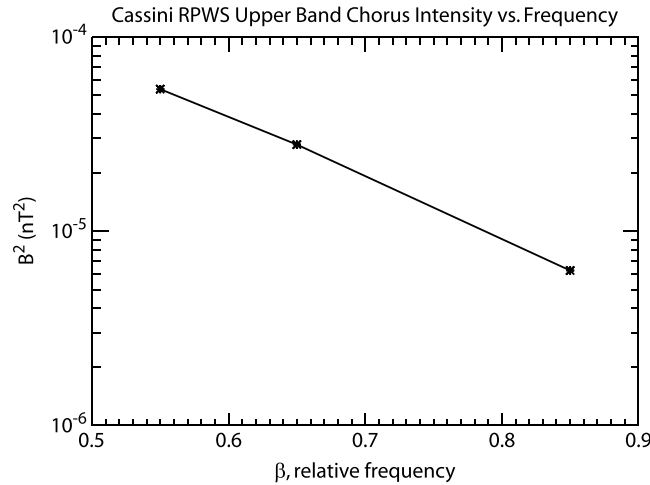


**Figure 9.** Average upper band chorus intensity versus  $\beta = fl/f_{ceq}$ . With only four points for the highest bin of  $\beta$ , no Gaussian fits were obtained.

plasma injection regions with more intense chorus emission, we determine that the peak chorus intensity is seen to occur in the lower range of  $0.3 < \beta < 0.4$  at a lower value of  $\sim 3.8 \times 10^{-5} \text{ nT}^2$  (compare Figures 4 and 5).

Upper band chorus is rarely observed outside of plasma injection regions and contributes very little to the overall chorus power. The distribution is dominant in the equatorial plane and scattered in local time for the relatively few cases observed.

The confinement of the chorus to a narrow range of L shells is distinct from the Earth, where the range is reported as  $4 < L < 9$  for lower band and  $3 < L < 7$  for upper band (Figure 7) [cf. Meredith et al., 2012]. The reasons for this are not completely known but, in analogy to Earth, are likely due to the lower ratio of

$f_p/f_c$  and the availability of anisotropic electron phase space distributions which provide a free energy source near the magnetic equator where both linear and nonlinear wave generation mechanisms are more efficient [Church and Thorne, 1983; Omura et al., 2008]. In contrast to Earth, however, Saturn is a rotation-dominated, not a solar wind-driven magnetosphere, which may control the radial range of wave-particle interactions capable of generating chorus. Saturn is also unique in that there is an obvious bias to the generation of upper band chorus within plasma injection regions, which are typically composed of warmer plasma temperatures and smaller values of  $f_p/f_c$  compared to the surrounding plasma for those injections typically observed by the Cassini RPWS instrument [Hill et al., 2005; Menetti et al., 2008]. The reasons for this difference between Saturn and Earth should be investigated. As discussed by Omura et al. [2009], the gap between the upper and lower chorus bands can be explained by nonlinear damping at  $f_c/2$ , where the chorus phase and group velocities are equal. At Saturn, the most intense emission does not occur at the magnetic equator, as at Earth, but a few

A-D14-056-2

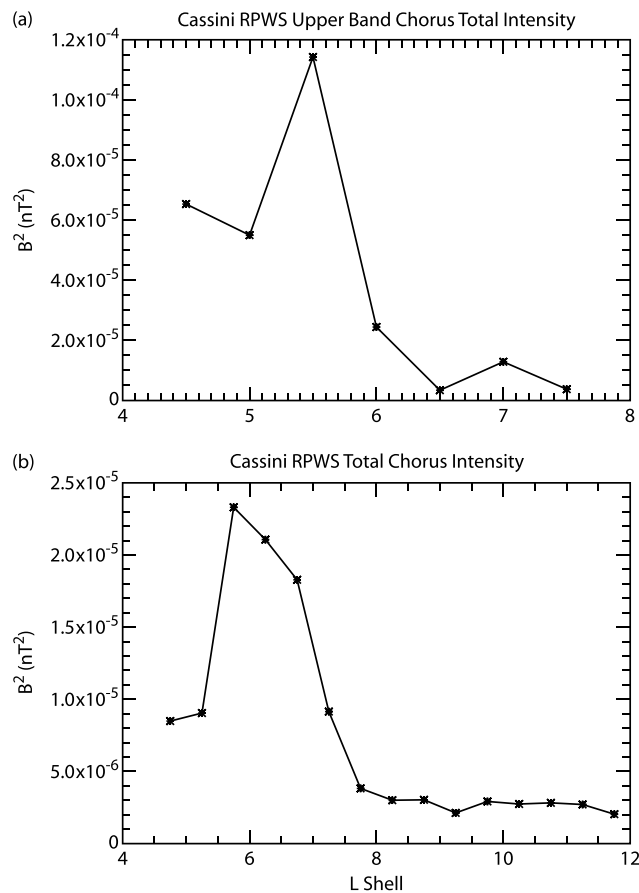


**Figure 10.** (a) Average chorus upper band intensity versus L (averaged in the same manner as for the lower band in Figure 7). Intensity levels are higher than for the lower band (Figure 7), but there are few source points. (b)  $P_{L,U}$ , the average magnetic intensity for both chorus bands is plotted versus L (note the difference in scales between Figures 10a and 10b).

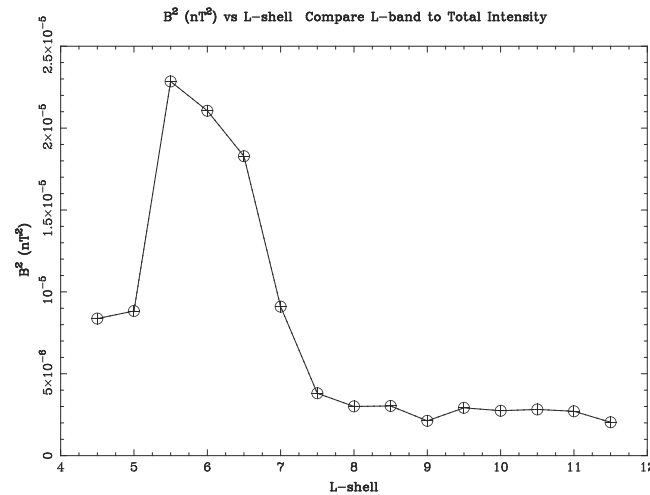


**Figure 11.** Average lower band chorus intensity (cross) and  $P_{L,U}$  (circles) versus L. The two curves are nearly identical, indicating that the upper band contributes little total intensity compared to the lower band.

degrees away from the equator, where nonlinear growth is observed [cf. Menietti et al., 2014]. At Earth, the upper band chorus is much weaker than the lower band [Meredith et al., 2012]; however, at Saturn, that is not the case as we have found (Figure 10). Another interesting fact is that upper band chorus will resonate with lower energy electrons than lower band. As these electrons drift out of the injection regions, they will resonate with lower frequency waves. It has yet to be shown how effective these waves are for electron acceleration at Saturn, compared to Jupiter and Earth [cf. Shprits et al., 2012].

Notably, the chorus intensity at Saturn is less than at Earth, but theoretical

models and simulations will be necessary to ascertain the effectiveness of Saturn chorus in electron acceleration and scattering in the radiation belts. A more careful study of the contribution of the total chorus intensity within injection regions to possible localized electron acceleration may be important.

**Acknowledgments**

We wish to thank J. Barnholdt for the administrative assistance and J. Christinger for the help with several figures. J.D.M. acknowledges support from JPL contract 1415150 and NASA grant NNX11AM36G. R.B.H. and E.E.W. are funded through STFC grant ST/1001727/1. R.B.H. is funded in the UK by NERC. Cassini RPWS data are archived in calibrated, full resolution at the NASA Planetary Data System website: <http://pds.nasa.gov/ds-view/pds/viewDataset.jsp?dsid=CO-V/E/J/S/SS-RPWS-3-RDR-LRFULL-V1.0>. The calibrated, full resolution WFR data are located at the same site: <http://pds.nasa.gov/ds-view/pds/viewDataset.jsp?dsid=CO-V/E/J/S/SS-RPWS-2-REFDR-WFRFULL-V1.0>.

Michael Liemohn thanks Rongxin Tang and another reviewer for their assistance in evaluating this paper.

**References**

Acuña, M. H., J. E. P. Connerney, and N. F. Ness (1983), The Z<sub>3</sub> zonal harmonic model of Saturn's magnetic field: Analyses and implications, *J. Geophys. Res.*, *88*(A11), 8771–8778, doi:10.1029/JA088iA11p08771.

Baker, D. N., et al. (2013), A Long-Lived Relativistic Electron Storage Ring Embedded in Earth's Outer Van Allen Belt, *Science*, *340*(6129), 186–190, doi:10.1126/science.1233518.

Burch, J. L., J. Goldstein, T. W. Hill, D. T. Young, F. J. Cray, A. J. Coates, N. Andre, W. S. Kurth, and E. C. Sittler Jr. (2005), Properties of local plasma injections in Saturn's magnetosphere, *Geophys. Res. Lett.*, *32*, L14502, doi:10.1029/2005GL022611.

Chen, Y., and T. W. Hill (2008), Statistical analysis of injection/dispersion events in Saturn's inner magnetosphere, *J. Geophys. Res.*, *113*, A07215, doi:10.1029/2008JA013166.

Church, S. R., and R. M. Thorne (1983), On the origin of plasmaspheric hiss: Ray path integrated amplification, *J. Geophys. Res.*, *88*, 7941–7957, doi:10.1029/JA088iA10p07941.

Connerney, J. E. P., N. F. Ness, and M. H. Acuña (1982), Zonal harmonic model of Saturn's magnetic field from Voyager 1 and 2 observations, *Nature*, *298*, 44–46, doi:10.1038/298044a0.

Connerney, J. E. P., M. H. Acuña, and N. F. Ness (1983), Currents in Saturn's magnetosphere, *J. Geophys. Res.*, *88*(A11), 8779–8789, doi:10.1029/JA088iA11p08779.

Glauert, S. A., and R. B. Horne (2005), Calculation of pitch angle and energy diffusion coefficients with the PADIE code, *J. Geophys. Res.*, *110*, A04206, doi:10.1029/2004JA010851.

Glauert, S. A., et al. (2014), Three-dimensional electron radiation belt simulations using the BAS Radiation Belt Model using new diffusion models for chorus, plasmaspheric hiss, and lightning-generated whistlers, *J. Geophys. Res. Space Physics*, *119*, 268–289, doi:10.1002/2013JA019281.

Gurnett, D. A., et al. (2004), The Cassini radio and plasma wave investigation, *Space Sci. Rev.*, *114*(1–4), 395–463, doi:10.1007/s11214-004-1434-0.

Gurnett, D. A., et al. (2010), A plasmopause-like density boundary at high latitudes in Saturn's magnetosphere, *Geophys. Res. Lett.*, *37*, L16806, doi:10.1029/2010GL044466.

Hill, T. W., A. M. Rymer, J. L. Burch, F. J. Cray, D. T. Young, M. F. Thomsen, D. Delapp, N. Andre, A. J. Coates, and G. R. Lewis (2005), Evidence for rotationally driven plasma transport in Saturn's magnetosphere, *Geophys. Res. Lett.*, *32*, L14510, doi:10.1029/2005GL022620.

Horne, R. B., R. M. Thorne, S. A. Glauert, J. D. Menietti, Y. Y. Shprits, and D. A. Gurnett (2008), Gyro-resonant electron acceleration at Jupiter, *Nat. Phys.*, *4*(4), 301–304, doi:10.1038/nphys897.

Hospodarsky, G. B. T., F. Averkamp, W. S. Kurth, D. A. Gurnett, J. D. Menietti, O. Santolík, and M. K. Dougherty (2008), Observations of chorus at Saturn using the Cassini Radio and Plasma Wave Science instrument, *J. Geophys. Res.*, *113*, A12206, doi:10.1029/2008JA013237.

Hospodarsky, G. B., K. Sigsbee, J. S. Leisner, J. D. Menietti, W. S. Kurth, D. A. Gurnett, C. A. Kletzing, and O. Santolík (2012), Plasma wave observations at Earth, Jupiter, and Saturn, in *Dynamics of the Earth's Radiation Belts and Inner Magnetosphere*, *Geophys. Monogr. Ser.*, vol. 199, edited by D. Summers et al., pp. 415–430, AGU, Washington, D. C., doi:10.1029/2012GM001342.

Kennel, C. F., and F. Engelmann (1966), Velocity Space Diffusion from Weak Plasma Turbulence in a Magnetic Field, *Phys. Fluids*, *9*, 2377–2388, doi:10.1063/1.1761629.

Kennelly, T. J., J. S. Leisner, G. B. Hospodarsky, and D. A. Gurnett (2013), Ordering of injection events within Saturnian SLS longitude and local time, *J. Geophys. Res. Space Physics*, *118*, 832–838, doi:10.1002/jgra.50152.

Li, W., J. Bortnik, R. M. Thorne, and V. Angelopoulos (2011), Global distribution of wave amplitudes and wave normal angles of chorus waves using THEMIS wave observations, *J. Geophys. Res.*, *116*, A12205, doi:10.1029/2011JA017035.

Menietti, J. D., O. Santolík, A. M. Rymer, G. B. Hospodarsky, A. M. Persoon, D. A. Gurnett, A. J. Coates, and D. T. Young (2008), Analysis of plasma waves observed within local plasma injections seen in Saturn's magnetosphere, *J. Geophys. Res.*, *113*, A05213, doi:10.1029/2007JA012856.

- Menietti, J. D., Y. Y. Shprits, R. B. Horne, E. E. Woodfield, G. B. Hospodarsky, and D. A. Gurnett (2012), Chorus, ECH, and Z mode emissions observed at Jupiter and Saturn and possible electron acceleration, *J. Geophys. Res.*, *117*, A12214, doi:10.1029/2012JA018187.
- Menietti, J. D., G. B. Hospodarsky, Y. Y. Shprits, and D. A. Gurnett (2014), Saturn chorus latitudinal variations, *J. Geophys. Res. Space Physics*, *119*, 4656–4667, doi:10.1002/2014JA019914.
- Meredith, N. P., R. B. Horne, A. Sicard-Piet, D. Boscher, K. H. Yearby, W. Li, and R. M. Thorne (2012), Global model of lower band and upper band chorus from multiple satellite observations, *J. Geophys. Res.*, *117*, A10225, doi:10.1029/2012JA017978.
- Omura, Y., Y. Katoh, and D. Summers (2008), Theory and simulation of the generation of whistler-mode chorus, *J. Geophys. Res.*, *113*, A04223, doi:10.1029/2007JA012622.
- Omura, Y., M. Hikosima, Y. Katoh, D. Summers, and S. Yagitani (2009), Nonlinear mechanisms of lower-band and upper-band VLF chorus emissions in the magnetosphere, *J. Geophys. Res.*, *114*, A07217, doi:10.1029/2009JA014206.
- Persoon, A. M., et al. (2009), A diffusive equilibrium model for the plasma density in Saturn's magnetosphere, *J. Geophys. Res.*, *114*, A04211, doi:10.1029/2008JA013912.
- Reeves, G. D., et al. (2013), Electron Acceleration in the Heart of the Van Allen Radiation Belts, *Science*, *34*(6149), 991–994, doi:10.1126/science.1237743.
- Rymer, A. M., et al. (2009), Cassini evidence for rapid interchange transport at Saturn, *Planet. Space Sci.*, *57*(14-15), 1779–1784, doi:10.1016/j.pss.2009.04.010.
- Santolik, O., D. A. Gurnett, and J. S. Pickett (2003), Spatio-temporal structure of storm-time chorus, *J. Geophys. Res.*, *108*(A7), 1278, doi:10.1029/2002JA009791.
- Shprits, Y. Y., R. M. Thorne, R. B. Horne, and D. Summers (2006), Bounce-averaged diffusion coefficients for field-aligned chorus waves, *J. Geophys. Res.*, *111*, A10225, doi:10.1029/2006JA011725.
- Shprits, Y. Y., J. D. Menietti, X. Gu, K.-C. Kim, and R. B. Horne (2012), Gyro-resonant interactions between the radiation belt electrons and whistler mode chorus waves in the radiation environments of Earth, Jupiter, and Saturn, a comparative study, *J. Geophys. Res.*, *117*, A11216, doi:10.1029/2012JA018031.
- Thorne, R. M., E. J. Smith, R. K. Burton, and R. E. Holzer (1973), Plasmaspheric hiss, *J. Geophys. Res.*, *78*(10), 1581–1596, doi:10.1029/JA078i010p01581.
- Thorne, R. M., et al. (2013), Evolution and slow decay of an unusual narrow ring of relativistic electrons near L ~ 3.2 following the September 2012 magnetic storm, *Geophys. Res. Lett.*, *40*, 3507–3511, doi:10.1002/grl.50627.
- Woodfield, E. E. R., B. Horne, S. A. Glauert, J. D. Menietti, and Y. Y. Shprits (2013), Electron acceleration at Jupiter: Input from cyclotron-resonant interaction with whistler-mode chorus waves, *Ann. Geophys.*, *31*, 1619–1630, doi:10.5194/angeo-31-1619-2013.
- Woodfield, E. E. R., B. Horne, S. A. Glauert, J. D. Menietti, and Y. Y. Shprits (2014), The origin of Jupiter's outer radiation belt, *J. Geophys. Res. Space Physics*, *119*, 3490–3502, doi:10.1002/2014JA019891.